REPORT DOCUMENTATION PAGE

Form Approved
OMB NO. 0704-0188

1. AGENCY USE ONLY *(Leave blank)*	2. REPORT DATE April 30, 2004	3. REPORT TYPE AND DATES COVERED Final 08/01/01 – 12/31/03

4. TITLE AND SUBTITLE

Coupled Asymmetric Quantum Dot (CAD) Laser

5. FUNDING NUMBERS

DAAD19-00-1-0483

6. AUTHOR(S)

J. S. Harris

7. PERFORMING ORGANIZATION NAMES(S) AND ADDRESS(ES)

Stanford University
328 CISX 4075
Stanford, CA 94305--.

8. PERFORMING ORGANIZATION REPORT NUMBER

9. SPONSORING / MONITORING AGENCY NAME(S) AND ADDRESS(ES)

U.S. Army Research Office
P.O. Box 12211
Research Triangle Park, NC 27709-2211

20040514 039

40372.1-EL

11. SUPPLEMENTARY NOTES

12a. DISTRIBUTION / AVAILABILITY STATEMENT

Approved for public release; distribution unlimited.

12 b. DISTRIBUTION CODE

13. ABSTRACT *(Maximum 200 words)*

Semiconductor solid-state lasers based on conduction-valence band recombination are now commonplace for low-power red emission, and are available commercially at nearly continuous wavelengths throughout the near-UV and near-IR communications bands. Furthermore, new lasers and broadband spontaneous emission sources are available through a wide wavelength range, including 3-8μm based on both conduction-valence band and intersubband transitions, and up to 70μm using cascaded intersubband transitions. However, competing processes make the design of these semiconductor lasers extremely difficult when extended to the very long, 300μm wavelength regime corresponding to low terahertz frequencies.

In this program, we have developed THz laser designs based on the intersublevel transitions in self-assembled quantum dots (QDs), where the lasing occurs through discrete conduction states. In an early implementation, two QDs are coupled to make a coupled-asymmetric quantum dot (CAD) laser similar to the quantum cascade laser but offering improved benefits. Unfortunately, current technological limits impede the fabrication of this device. In another scheme, an ensemble of non-coupled QDs is selectively placed in a high quality cavity, called a microdisk, which is resonant with an intersublevel QD transition. In this program, we have demonstrated the initial fabrication of this structure.

14. SUBJECT TERMS

15. NUMBER IF PAGES
29

16. PRICE CODE

17. SECURITY CLASSIFICATION OR REPORT UNCLASSIFIED	18. SECURITY CLASSIFICATION OF THIS PAGE UNCLASSIFIED	19. SECURITY CLASSIFICATION OF ABSTRACT UNCLASSIFIED	20. LIMITATION OF ABSTRACT UL

1. List of manuscripts:
   a. G. S. Solomon, M. Pelton, and Y. Yamamoto, "Single-mode Spontaneous Emission from a Single Quantum Dot in a Three-dimensional Microcavity," Phys. Rev. Lett. **86** (17) 23 April 2001. 3903-3906.
   b. G. S. Solomon, "Competing Processes in the surface ordering of InAs islands using a subsurface island superlattice," Appl. Phys. Lett. **84** 2073, 2004.
   c. G. S. Solomon, *Coupling and ordering of quantum dots using InAs quantum dot multilayers,* accepted for publication in "Encyclopedia of Nanoscience and Nanotechnology," H. S. Nalwa, editor, American Scientific Publishers (2004).
   d. G. S. Solomon, Z. Xie, and M. Agrawal, *Terahertz Emission Using Quantum Dots and Microcavities*, accepted for publication in "Terahertz Sensing Technology" M. Shur, editor, World Scientific Publishing, Singapore (2003).
   e. G. S. Solomon, Z. Xie, W. Fang, J. Y. Xu, A. Yamilov, H. Cao, Y. Ma, and S. T. Ho, "Large spontaneous emission enhancement in InAs quantum dots coupled to microdisk whispering gallery modes," Phys. Stat. Sol. (b) **238**, 309 (2003).
   f. G. S. Solomon, M. Pelton, and Y. Yamamoto, Phys. Rev. Lett. **90** 229702 (2003).
   g. G. S. Solomon, M. Pelton, and Y. Yamamoto, "Spectral tuning of the coupling between isolated InAs quantum dots and the fundamental micropost cavity mode," Phys. Stat. Sol. (c), **0**, 1205 (2003).
   h. W. Fang, J. Y. Xu, A. Yamilov, H. Cao, Y. Ma, S. T. Ho and G. S. Solomon, "Large enhancement of spontaneous emission rates of InAs quantum dots in GaAs microdisks," *Opt. Lett.* **27**, 948 (2002).
   i. H. Cao, W. Fang, J. Y. Xu, A. Yamilov, Y. Ma, S.T. Ho, and G. S. Solomon, "Large enhancement of spontaneous emission rates of InAs quantum dots in GaAs microdisks" Technical Digest Summaries **1** p.56: Quantum Electronics and Laser Science Conference 19-24 May 2002, Long Beach, CA.
   j. H. Cao, K. J. Luo, J. Y. Xu, Y. Ma, G. S. Chang, S. T. Ho and G. S. Solomon, "Ultrafast dynamics of InAs/GaAs quantum dot microdisk lasers," *Tech. Digest Sum. Of Quant. Electron. and Laser Sci. Conf., Conf. Edition*, Baltimore, May (2001).

2. Scientific Personnel: (1) James Harris
   (2) Glenn Solomon
   (3) Zhigang Xie
3. Report of Inventions: none
4. Scientific Progress: see attached
5. Technology Transfer: none

J. S. Harris and G. S. Solomon

Department of Electrical Engineering, Stanford University

Stanford, CA

Table of Contents

1.0 Introduction

The terahertz (THz) frequency window has recently been of scientific, commercial, and military interest for a variety of reasons. While optical sources are available a frequencies greater than 10 THz, and electronic oscillator circuits are available at frequencies in the 500 GHz range, the THz band, for the purposes of this chapter between 0.8-3 THz, remains elusive. The region is conceptually interesting because of the overlap of sources and technologies from the optical and electronic domain. From a solid-state physics perspective, there is a growing interest in THz spectroscopy for research in fundamental band structure [1], excitonic physics [2] and multi-particle states such as Bose-Einstein Condensation and quantum liquids [3]. In chemistry and biology there is interest in low THz sources (1 THz) for molecular detection [4]. The frequency regime is also of technological interest such as THz-band communications. New military sensing capabilities, including radar and spectroscopic sensing, will be developed in the THz frequency range. New spectroscopic sensing can be used effectively to enhance security. Finally, sources emitting in this region can used in medical imaging and biological sensing.

One type of source will not meet all these needs, but needs fall into two or three categories. First, a coherent source of sufficient power is necessary. In some instances an electronic circuit with a THz-resonant local oscillator is desired, while in other circumstances an optically based source, such as a laser is more applicable. In both cases power in the milliwatt (mW) range is more than likely necessary. Finally, a broadband source will be useful for spectroscopy. While spectroscopic needs can be met with a series of well-designed lasers, in some situations where lower power is acceptable, a broadband source will be more effective.

In this program we have developed two new schemes for terahertz emission. Both focus on semiconductor quantum dots (QDs). One scheme is related to the quantum cascade laser but is based on QDs in-place of quantum wells. The QDs should limit losses such as those related to phonons and provide better radial emission properties. The second scheme uses QDs but recognizes that because the optical wavelengths are so long in the terahertz, if a high-quality optical cavity is used to enhance optical feedback for lasing, it must be designed in the plane of the semiconductor. In this scheme a microdisk cavity is used and the QDs must be placed in the narrow cavity mode at the disk perimeter. For this we develop and novel approach to QD placement using molecular-beam epitaxy and processing. Before we discuss these schemes and results we develop background that motivates this work.

Semiconductor-based solid-state lasers and light-emitting diodes (LEDs) are ubiquitous. These sources typically operate near the visible spectral range, at wavelengths between 400 nm out to a few microns, although there are sources available at shorter and longer wavelengths. What limits the emission wavelength and what can be done to bring the emission wavelength out to the 100 μm to 300 μm THz regime? There are two general categories that conspire to reduce the emission efficiency in both the UV and far IR that are based on the solid-state nature of the lasing material: competing

parasitic processes and poor material properties. Completing parasitic processes, such as free-carrier absorption and Auger recombination in long wavelength sources, and highly electrically resistive layers in short wavelength sources are generally intrinsic, while poor materials properties are technology related. The most mature optoelectronic material system, based on GaAs, turns out to have significantly advantageous materials properties, in part because of years of development, but also because of available lattice matched alloys with good refractive index contrast and bandgap differences, and relatively easily produced substrates.

Take as an introductory example the case of UV lasing based on, for example GaN. Since the transition energy is large (UV), the bandgap or heterostructure band offsets also must be large. Typically, the optically active transitions occur in quantum wells (QWs), which have more favorable density of states, thus, the QW barrier materials must have even larger bandgaps. The crystal growth processes are very difficult in these wide bandgap semiconductors because good substrates are not available and there is typically a significant lattice mismatch between alloys, making heterostructures with large confinement difficult to fabricate. In many material systems it is difficult to find stable regions in the crystal growth parameter space where materials can be successfully deposited, either do to phase segregation or excessively high vapor pressure at ideal growth temperatures. Furthermore, the index contrast between nearly lattice-matched materials is small, making waveguiding difficult. Finally, because the bandgaps are large, the intrinsic carrier concentration is low and high activated doping levels are difficult to achieve, resulting in more highly resistive structures and poor electrical contacts.

In contrast, for near-IR based devices, GaAs and InP are available. The excellent crystal growth technologies developed around GaAs and InP has been fortuitous for sources emitted in the visible to near IR. Despite being some of the first compound semiconductors investigated, the excellent crystal growth properties are rather unique. While Si is unique in the formation of a stable, high quality oxide, GaAs and to some extent InP are unique in optical heterostructure devices. In the GaAs-AlAs system there is a favorable band offset which is over 50% of the GaAs bandgap, and yet the materials are nearly latticed matched with good index contrast.

For the narrow energy transitions used in long-wavelength lasers, either inter- or intraband transitions can be used. The same types of material issues are present here as in the wide bandgap materials. Lattice mismatch is often a problem, and index contrast is once again an issue. Now the materials' refractive indices become smaller with increasing operating wavelength. Furthermore, although it is not difficult to achieve the proper doping, excess carriers contribute to parasitic free-carrier absorption at long wavelengths. Besides free-carrier absorption, other processes become favorable at longer wavelengths. In the 30 meV (41.3µm) range optical phonons are typically active in multi-atom basis crystals, and multi-particle processes, such as Auger recombination also become more significant.

In the near to mid-IR, where free-carrier absorption is still a small parasitic there is a competition between interband and intraband lasers. The general problems with interband lasers are the competing process of Auger recombination, and the crystal growth issues such as available substrates, lattice matching and alloy uniformity. As the interband energy reduces, Auger processes, becomes more favorable. The crystal growth problems are typical of those mentioned above with respect to both UV and IR devices. Such is the case for typical IR materials such as HgCdTe, where specially alloyed substrates of the $Cd_{0.96}Zn_{0.04}Te$ are necessary to minimize the lattice mismatch [5]. Furthermore, controlling the alloy uniformity has been difficult. However, lasers are made and will continue to improve, although the pace has been slow compared to GaAs and InP. Operating at 2.6 µm, edge emitting devices with threshold current densities of 420 A/cm^2 have been achieved on approximately 800 µm long structures under pulsed conditions at 77K [5]. Parallel to these efforts has been the intraband based structures using either GaAs- or InP-based material systems. These efforts leverage the successes of these materials system at shorter wavelengths along with those of quantum well (QW) physics. These are truly artificially structured crystals, where the transition energies and rates are determined by designing barrier heights and QW widths to tune individual QW wavefunctions. For lasers, the result of these efforts has been the cascade lasers [6]. These devices are unipolar, typically utilizing the conductor band, and can in principle operate through the electromagnetic spectrum except for the previously raised issues of competing parasitic processes and index contrast.

A terahertz optical emission source is proposed here that will offer both broadband spontaneous emission and lasing for a variety of needs in the THz frequency regime. The source is based on the emission from a quantum dot (QD) active region to reduce non-radiative loss and which can be coupled to a high quality optical cavity. The THz source can be optically pumped with a low power, compact laser source, or electrical injection can be implemented.

In one implementation two layers of QDs are quantum mechanically coupled by tuning the size/shape of the QDs in each layer. We call this structure a Coupled Asymmetric Dot (CAD) laser. It directly addresses the problem of the removal of carriers from the ground state of the optical transition. In a different device, the emphasis is on creating a high quality waveguide to either focus broadband emission or to allow feedback and gain for lasing, and uses a microdisk cavity. In the microdisk, cavity modes are present at the circumference of the disk containing the QDs. These circumferential modes, called whispering gallery modes, exist due to total internal reflection from the disk sidewalls. Because the device emits in-plane, thick vertical layers of material are not necessary, easing fabrication. QD emission that is coupled to these optical modes can be guided and extracted from the device.

Other sources have recently become available in the THz regime. A quantum cascade laser source has been made in the THz regime [7]. Other sources approaching, but not achieving THz emission frequencies have been demonstrated in the electronic domain [8]; however, clear demonstration of THz emission has not, to our knowledge, been

demonstrated in the electronic domain, and it is unlikely these sources will provide the coherent emission power of a laser.

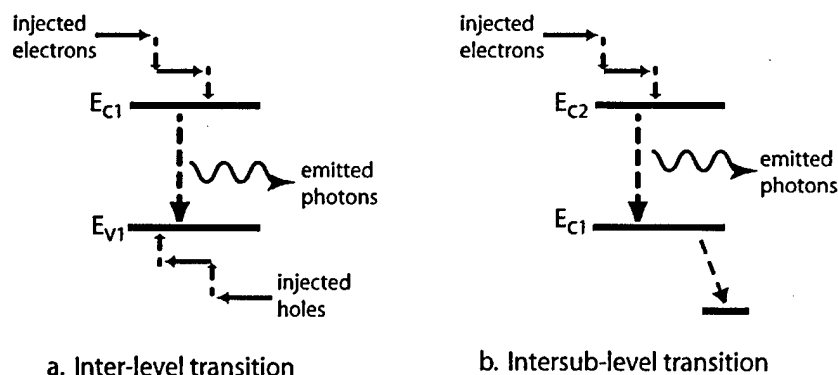a. Inter-level transition   b. Intersub-level transition

Fig. 1. Energy band diagram of interband transition (a), and intersubband transition (b) under carrier injection. Electrons and holes must be injected in the interband transition, and the ground state is the annihilation of carriers. Intersubband radiative transitions are unipolar, but the lower state of the transition is occupied by carriers which must be removed through another transition.

2.0 The Terahertz Emission Regime

Here, we discuss three particular issues that are important in long-wavelength optoelectronic sources. These are (1) the long-wavelength active region; (2) losses particular to the ultra long wavelength regime; and (3) materials and fabrication issues associated with device geometry of long-wavelength sources.

2.1 THz emission sources.

Two possible THz emission/absorption active regions are available: *Interband, i.e.,* direct bandgap transitions and *intraband* (which we prefer to call *intersubband*), *i.e.,* transitions in quantum-confined structures between confined conduction or valence states. These transitions are shown in Fig. 1. For direct bandgap, interband transitions in the THz regime a near zero bandgap semiconductor is required. For intersubband transitions more conventional wider bandgap materials can be used, but require precise, often completed structures. The wavefunctions of the crystal can be written as Bloch functions, $\Psi = u(k,r)e^{ik \cdot r}$, where $u(k,r)$ is the basis function, with periodicity on the order of the crystal lattice and $e^{ik \cdot r}$, is the envelope function. For an optical transition in the crystal, under the assumptions of a weak electromagnetic field and where the photon momentum is small compared to the crystal momentum, the Hamiltonian is the momentum operator, $i\hbar\nabla$. This derivative operator necessitates that for non-zero transitions the initial and final wavefunctions must have a non-zero inner product. The interband transition is a transition between two bands with orthogonal basis states and overlapping envelope states, such as the conduction band and valence band transition,

shown in Fig. 1a. If the transition is intersubband the basis states overlap and the envelope states are orthogonal.

In Fig. 2 schematics of the band structure of the direct bandgap transition in bulk semiconductor (Fig. 2a) and the intersubband transition in a quantum well (QW) structure are shown (Fig. 2b), where the curly lines represent photon emission. In Fig. 2a the density of states in conduction and valance bands are continuous, while in Fig. 2b a QW structure is shown having discrete jumps in the density of states due to subband formation in conduction and valence bands. The direct bandgap transition can be used in either bulk material, shown, or with a QW. Indeed, in most applications a QW will be used. Again, the intersubband transition *requires* quantum confinement since the subbands form from the confinement.

While direct bandgap structures are in concept simple and the output power often higher than intersubband structures, there are increased intrinsic losses in these structures. The materials development of these very narrow bandgap semiconductors is in its infancy. If the development of mid IR interband sources is any guide, THz interband sources will have a significant development period.

Intersubband transitions overcome a large portion of the Auger and inter-valance band absorption losses (both discussed below) associated with long wavelength direct bandgap structures. QWs can be made with high precision using well-established materials, typically GaAs or InP, and the transition energies can be tuned through the well-developed molecular-beam epitaxy (MBE) growth process. The MBE process has local (100 µm) resolution on the order of a monolayer (2.5Å) in the crystal growth direction. However, the transition strengths from intersubband band transitions are typically lower than direct bandgap transitions, reducing the output power. Even though the dipole strength is typically larger than in direct bandgap transitions, because the spatial extent of the envelope states, the overall overlap integral between the states is often less.

There are also addition design constraints in intersubband structures. In many cases, for example symmetric QWs, normal emission or absorption is forbidden. Also, the optical transitions involve carriers from a single band; the transitions are thus unipolar. In unipolar, intersublevel devices carriers transition from the upper radiative state to the lower radiative state. Conduction band electrons do not recombine with valence band holes as in interband transitions, and thus a population of lower state carriers remains. If the decay of the lower state population is not sufficient the quasi-equilibrium population will reduce the density of available lower states, clamping the radiative decay process. Thus, the intersublevel QD (or QW) emission source must be designed in a way that reduces the ground state quasi-equilibrium occupation. An addition decay path is shown from the lower emission state in the intersubband diagram in Fig. 1b.

As of June 2002, the cascade laser does provide emission in the THz regime [6]. The laser operates at 3 THz with an output power of 1 mW at 40K. THz emission has not been demonstrated from a direct bandgap transition in a narrow bandgap semiconductor. Indeed, the cascade laser has been a major achievement, the result of over a decade of

focused research. The structure is complicated and can only be made at long wavelengths in a small number of laboratories worldwide.

2.2 Free carrier, phonon, Auger and intervalence band absorption losses

One of the most difficult problems in designing long wavelength sources is the increase in absorption and parasitic recombination related losses. These losses increase nearly exponentially with increasing wavelength as schematically illustrated in Fig. 3. Free-carrier absorption is not in-principle limited to a single band, but for the purposes of our discussion we will limit it to a single band. This is especially relevant because of our focus on low-energy, THz absorption. Since the momentum of each carrier is uniquely defined within a band except for spin degeneracy, and the photon momentum is negligibly small compare to the crystal momentum, the intraband free carrier absorption necessities an additional momentum scattering interaction. Additional scattering could include lattice scattering (phonon) or impurity scattering. Also, necessary is a partially
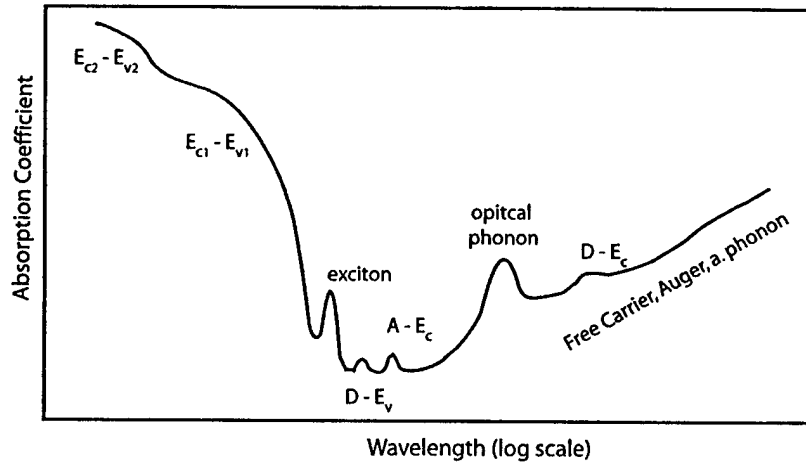

Fig. 3. Schematic of absorption as a function of wavelength indicating the increasing effect of free-carrier absorption at long wavelengths. E_c-E_v is the conduction-to-valence band transition (two bands are shown), while D, A are donor and acceptor levels. (Not to scale.)

filled band. In the semi classical picture, the electric field of the incident radiation accelerates the free carriers in a band, which are eventually decelerated by scattering. If the scattering is from the lattice, the energy is converted to heat. Thus, from this semi classical picture the free carrier absorption is related to the high-frequency conductivity [9,10]

$$\sigma = \sum_i q^2 \frac{n_i}{m_i^*} \tau_i^* = \sum_i q^2 \frac{n_i}{m_i^*} \left\{ \left\langle \frac{\tau_m}{1+\omega^2\tau^2} \right\rangle - i\omega \left\langle \frac{\tau_m^2}{1+\omega^2\tau^2} \right\rangle \right\},$$

where q is the charge of the carrier in the ith band, n is the carrier concentration, m^* is the effective mass in the ith band, τ^* is the effective relaxation time, defined as a function of

the incident frequency, ω and the relaxation time, τ_m. For free-carrier absorption where a photon is absorbed by an electron in the lowest conduction band or hole in the highest valence band the absorption becomes

$$\alpha_c = \left(\frac{\lambda^2 q^3}{4\pi^2 c^3 n_r \varepsilon_0} \right) \left[\left(\frac{n}{m_c^2 \mu_c} \right) + \left(\frac{p}{m_h^2 \mu_h} \right) \right],$$

where λ is the wavelength,, n_r is the refractive index, ε_0 is the vacuum dielectric constant, n (p) is the electron (hole) concentration in the conduction (valance) band, μ is the conductivity carrier mobility ($\mu_i = q\tau_{m,i}/m_i$). A quantum mechanical treatment [11] confirms the semi classical picture when $h\omega < kT$ (or E_F). The process is depicted schematically in Fig. 4 below. Free carrier absorption becomes increasingly important at long wavelengths, increasing with the square of the wavelength. Since n (p) is

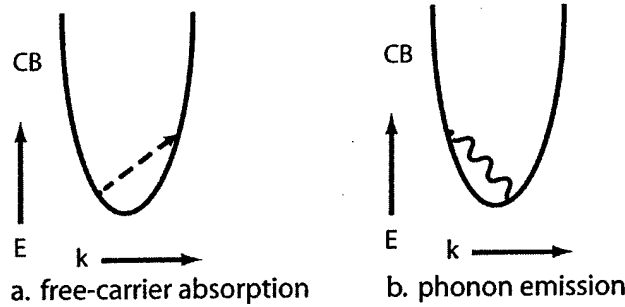a. free-carrier absorption   b. phonon emission

Fig. 4. Free-carrier absorption within a single bulk band is shown in (a), where the transition is k-conserving. In (b) a phonon emission is shown, reducing the energy of the electron. This transition is not necessarily k conserving.

proportional to $m^{3/2}$, the bracketed terms are proportional to $m^{1/2}$, making the effect of holes larger for similar τ. In narrow bandgap structures, where the conduction band electron mass is typically smaller than in wider bandgap materials, the free carrier absorption due to conduction electrons is slightly reduced, but the λ^2 is the dominant feature as seen in Fig. 3. In interband structures made of wider bandgap materials, free-carrier absorption is reduced because of increased restrictions on allowed momentum in the confinement direction.

Phonon absorption or emission losses involve an electron or hole, and an absorbed or emitted phonon, and do not require momentum conservation. Phonon emission with the relaxation of an electron is shown in Fig. 1,2b. While the emission of a phonon can occur at any temperature, phonon absorption requires the presence of a phonon population, which is given by Bose statistics. The optical phonon (LO) has a peak energy in its dispersion ~ 30-50 meV at $k=0$. The acoustic and optical phonon branches are continuous except for a small energy gap near the Brillouin zone edge. For GaAs the k=0, LO phonon energy is 32 meV, or just into the THz regime. Thus, when band structure of the system is designed around this energy to produce direct bandgap THz

radiation, the energies are also close to the LO phonon, $k=0$ resonance, dramatically reducing THz photon emission.

While the free-carrier and phonon absorption processes are not momentum conservation, the Auger and intervalence band absorption process involve are at least three particle processes to conserve momentum. Auger recombination can take many forms in semiconductor materials. An example is an electron initially in the conduction band relaxing to a valance band hole state, and another electron in the conduction band moving to a higher conduction band state (Fig. 5a). Another Auger process is the recombination of an electron in the conduction band with a hole in the valance band and the relaxation of a hole deeper in the conduction band (Fig. 5b). In these processes, the
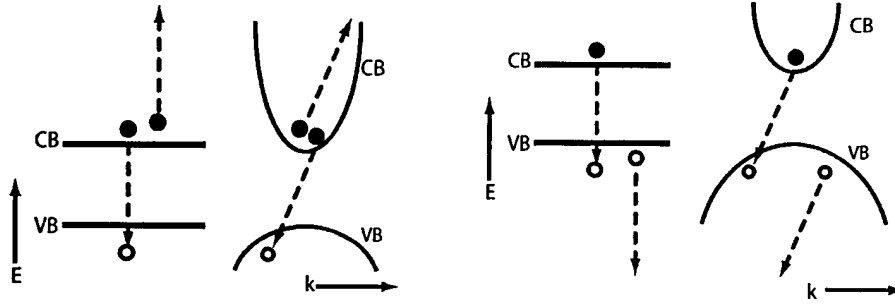

Fig. 5. Energy and energy-momentum diagrams showing two common Auger processes in narrow bandgap semiconductors. In (a), an electron in the conduction band (CB) relaxes to the valance band (VB) and the energy and momentum is converted to exciting an electron in the CB. In (b) the energy from the electron relaxation process excites a hole deeper into the VB. Since these processes involve three particles, the transition rates are proportional to n^2p in (a), and np^2 in (b).

energy of the two transitions is equal and the total momentum is conserved. Note that here the relaxation from the conduction band is not k conserving and thus a photon could not be emitted without another particle interaction to conserve momentum.

Since these Auger processes involve three particles, the transition rates are proportional to the concentrations of all the carriers involved, i.e., n^2p in (Fig. 5a), and np^2 in (Fig. 5b), and can be represented in the form [12]:

$$R_{Auger} = c(T)n^2p, \text{ where } c(T) = c_0\left(\frac{E_a}{kT}\right), \text{ with } E_a = \frac{m_cE_g}{m_c + m_h}$$

where the Auger process is represented in Fig. 5a. The constant c_0 is a function of the dielectric constant, and m_c and m_v . The value of E_a depends of the details of the multiparticle process and there is some discrepancy [9,12] on the form of E_a. From the above equation as the bandgap narrows the Auger process increases exponentially. The process is further enhanced by the generally smaller electron mass in narrow bandgap materials.

Finally, intervalence band absorption (IVBA) processes are important when there are valance band energy differences that are less than the wavelength of emitted light. The valance band is composed of heavy and light hole bands, which are degenerate in cubic

9

bulk semiconductors, and the spin split-off band. These processes are similar to free carrier absorption, and correspond to transitions between subbands in the valance band.

We would like to make two important points associated with the losses discussed. First, losses that are relatively minor, but still can impact device performance in the near IR such as Auger recombination, can dominate fundamental device processes in long-wavelength, THz devices. Second, QW confinement can usually reduce these effects.

2.2 Materials, fabrication and geometry issues in THz devices.

With wavelengths on the order of 30-300 μm, active regions, waveguide and cavity designs, and general device layout must be considered. In many ways, these long wavelengths offer relaxed processing accuracy; however, when vertical components are a necessary feature in the device design the crystal growth process becomes expensive, time consuming and variable. For example, vertical cavity surface emitting lasers (VCSELs) in the THz regime are not realistically possible. With half-wavelength cavities and mirror pairs numbering over 30, the overall vertical size is on the order of 150 μm and would take over 100 hours to make by molecular-beam epitaxy (MBE). However, good cavities are needed for these devices to overcome the large losses
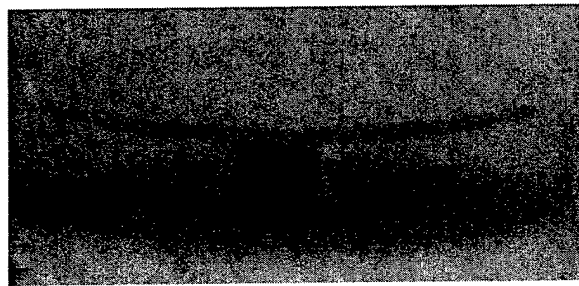

Fig. 6. GaAs/AlGaAs microdisk cavity make by the authors. The cavity mode is on the perimeter of the disk [13].

previously discussed. Thus, a high-quality in-plane cavity is necessary. For this purpose we use a microdisk cavity. This cavity possesses the very high quality factors necessary for THz emission, yet the in-plane geometry of the microdisk reduces materials costs and time, and simplifies fabrication. A scanning-electron microscope (SEM) image of such a cavity is shown in Fig. 6. For THz emission the in-plane cavity diameter will be approximately 100 μm and the height will be 5 μm (for 6 THz). The large in-plane diameter simplifies fabrication while the height is very reasonable for any crystal growth process.

3.0 QD and Cavities as Terahertz Sources

We have made a case for the use of intersubband transitions for THz emission, instead of the direct bandgap transitions in narrow bandgap materials. While the choice

of either interband or intersubband structures is not obvious for mid-IR applications, the choice is much more obvious in terahertz applications. While several mid-IR direct bandgap materials are under development for many years for interband devices, there is no such terahertz material. If the development of interband materials begins in the terahertz range, it will require substantial development lead time. In direct narrow bandgap materials the material control is poor and the intrinsic losses large. For intersubband transitions standard materials can be used and the epitaxial control that has been developed over the last two decades can be leveraged to produce well-engineered structures. Furthermore, the losses, so problematic in long-wavelength devices are reduced in the structures.

What is gained by further reducing the system dimensionality from the 1-dimensional confinement of QWs to the 3-dimensional confinement of QDs? First, the QD structure does provide reduced losses in the categories discussed in Section 2.2. While LO phonon absorption is inhibited at frequencies below 8 THz, free carrier absorption and Auger recombination are prominent, as well as acoustic phonon absorption at longer wavelengths. These losses are reduced in intersubband structures because of the reduced dimensionality in momentum space; however, these losses are not eliminated as there remains many possible available transitions. However, in QDs, with their atomic-like transitions, there is no crystal momentum dispersion in the band structure, putting sever restrictions on the losses discussed in Section 2.2. This can be seen in Fig. 7. An additional advantage of QD THz emitters is the relaxed non-normal emission requirements associated with QWs.

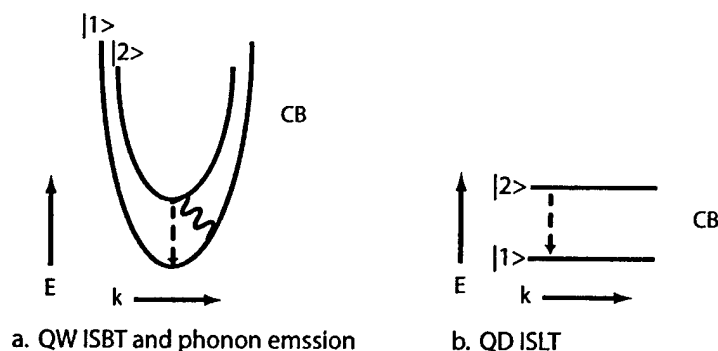
a. QW ISBT and phonon emssion   b. QD ISLT

Fig. 7. Intersubband recombination processes and the band structure of a QW and QD are compared. (a) Radiative and nonradiative (phonon) relaxation processes in intersubband transitions (ISBT) in a QW. Because there is a distribution of energy differences between the two subbands, there is likely a match to the energy. (b) Because there is no momentum dispersion, the intersublevel transition (ISLT) has a fixed energy and is likely not to correspond to the phonon energy.

In certain promising geometries QWs simply will not function optimally. QWs and bulk materials are not particularly compatible with many nanostructures because of the nonradiative recombination that occurs at free surfaces. Bulk-crystal band structure is based on an effectively infinite crystal with no surface effects. Free surfaces are

discontinuities in bulk materials, the causing breaking of the crystal symmetry and modified local bonding (surface reconstruction), and thus create new 'surface states.' Nearly all surfaces have surface states, and a large number of these states exist in the energy gap of band structures, creating band bending and recombination sites for carriers. Because of their 3-dimensional confinement, QDs can be uniquely isolated from free surfaces with minimal effort while still remaining spatially close to these surfaces. The microdisk cavity is one such nanostructure (Fig. 6). The cavity mode is very close to the microdisk edge and nonradiative recombination can become a parasitic in the critical active region. Towards the center of the disk, away from the cavity region there is no surface recombination, but any QW recombination in this region is poorly coupled to the cavity mode. With QDs in the cavity mode, carriers diffuse from the pumping region to the QDs at the microdisk edge where they recombine without nonradiative surface recombination.

Like QWs, optical emission can occur in QDs through either interband or intersubband transitions. Since there is no *band* is the QD electronic structure we often use *level*, such as an intersublevel transition, but for convenience also often retain the band usage. However, just like interband structures formed from direct bandgap materials, interlevel, conduction to valence state QD transitions in the THz regime requires tuning the QD confined conduction and valence state differences to below 20 meV (5 THz). Any substantial quantum confinement will be on the order of 10-20 meV, implying the QD material bandgap must be near zero. While semimetals with bandgaps of 10 meV are possible, as mentioned above the materials growth technologies will be substantial. Thus, our structures will be based on intersublevel QD transitions.

As in QWs, designing a QD, or ensemble of QDs with an intersublevel transition is in principle not difficult. However, in unipolar, intersublevel devices carriers transition from the upper radiative state to the lower radiative state. Since the structure is unipolar, conduction band electrons do not recombine with valence band holes, and thus a population of lower state carriers remains. If the decay of the lower state population is not sufficient the quasi-equilibrium population will reduce the density of available lower states, clamping the radiative decay process. Thus, the intersublevel QD (or QW) emission source must be designed in a way that reduces the ground state quasi-equilibrium occupation.

While QDs active regions can provide reduced losses and can be integrated into high performance cavities such as microdisk, current fabrication suffers from large inhomogeneous size distributions. Using crystal growth techniques such as MBE, QWs can be fabricated with precision because the critical confinement dimension is in the growth direction, where MBE has local, monolayer thickness control. However, for QDs two additional confinement dimensions are needed. First generation QD structures were fabricated from QW processed into QDs using lithography. However, these structures suffered from surface recombination due to defects associated with directly etching the active device region. An alternative approach was developed in the mid 1990s, and uses lattice mismatch strain to form heterostructure islands of quantum-size dimensions in a larger bandgap host. When a lattice mismatched material such as InAs is deposited on

host crystal such as GaAs (lattice mismatch~7%), the lattice mismatch strain is absorbed by the host as biaxial compression of the epitaxy (InAs). Since the InAs lattice constant is larger than the GaAs host, when a small amount of material is deposited it is compressed in-plane (biaxial compression), expanding in the growth direction according to Poisson's ratio, but remaining essentially planar. However, as more lattice mismatched material is deposited, the accumulated strain energy increases to a level where a different strain accommodation is energetically more favorable: the lattice mismatched epitaxy creates islands. These islands provide surface curvature to laterally relax the mismatched material. The crystal surface has excess bond energy compared to the interior of the crystal since the bonding environment of the bulk has been disturbed by the surface. Without the excess strain energy from the lattice mismatched epitaxy, the surface area would be minimized, minimizing the total crystal energy. However, as the total strain energy increases it is energetically more favorable to create more surface area to reduce the strain energy. The islands formed remain once covered by the host (although their shape may change) and if the proper materials are chosen, can be used as QDs. A layer of QDs has a large inhomogeneous size distribution because the local strain environment driving the process is not unique and is difficult (or impossible) to control. For example, InAs-based QDs are formed in a GaAs host with in-plane dimensions of 20-30 nm and vertical dimensions of 4-5 nm. Photoluminescence at 4K on isolated single QDs indicates linewidths on the order of 100 μeV, while the spectral linewidth of the full ensemble is typically 25 meV near the 1.3eV ensemble-average spectral peak emission.

Such a large QD ensemble linewidths is detrimental for three reasons. First, the emission efficiency is directly related to the density of optical emitters, and since losses are large in the THz, it is particularly important in these applications that the emitter density at the designed frequency is large. The designed spectral linewidth is rarely large. Second, to overcome losses and facilitate gain a high-quality optical cavity is used, which has a narrow resonance. Thus, to optimize coupling between the emission source
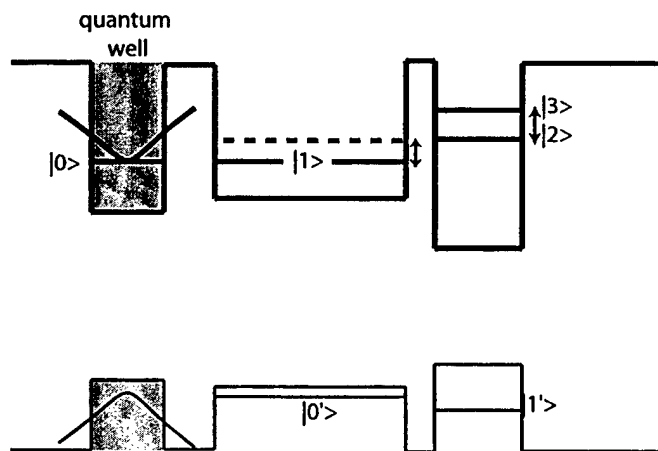

Figure 8. Schematic diagram of the band structure of the Asymmetric Coupled QD laser.

and the cavity the emission source should have a spectral linewidth on the order the spectral linewidth of the cavity. While microdisk cavities, for example, do not have resonances of 100 μeV they can be on the order 1000 μeV. The final problem with the size variation in strain-induced QDs is the inability to precisely tune the coupling between QDs in different layers. It has been shown [14] that layers of QDs separated by thin layers of the host crystal can be coupled. It is possible to observe this coupling for an individual coupled QD pair [15], but it is currently not possible to engineer this coupling for the entire ensemble because the QD size control is not precise. This last problem is particularly detrimental when designing QD intersublevel structures, since designing short lower radiative state lifetimes is important and is often accomplished in QW systems by coupling the lower state to another structure. Such is the case in the coupled-asymmetric quantum dot emission device described below. To realize this device, new QD fabrication techniques will be necessary.

4.0 The Coupled Asymmetric Quantum Dot (CAD) Laser

Our vision of an intersublevel QD laser employs a coupled asymmetric QD (CAD) structure. The band structure is shown in Figure 8. In this structure a large, QD will be deposited on top of a smaller dot by our vertical aligned QD column technique. The size of each QD will be controlled by adjusting the alloy composition. We have successfully used this technique to align up to 10 QDs of the same approximate alloy composition in vertical columns [16]. Three QD conduction energy levels will be used from these QDs to form the core portion of the THz laser. Lasing will occur between the excited state and ground state in the conduction levels of the smaller dot, and we denote this transition as |3>-|2>. Holes must be absent from this device in the first excited valence state or conduction-valence level radiative recombination from excited electron and hole states becomes a competing process. For fast relaxation out of the electron ground state (|2>)
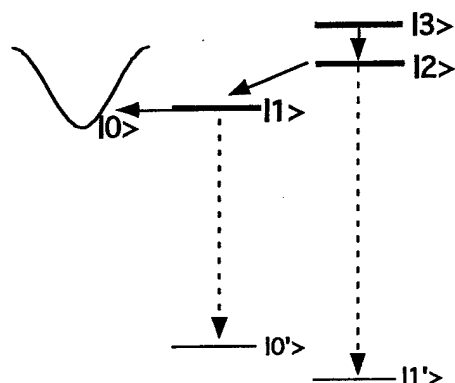

Figure 9. Radiative and nonradiative transitions involved in the lasing process are shown.

a second, larger QD will be used. Its electron energy level will be tuned an LO phonon away from the |2> level and will provide extremely fast relaxation for the ground state of the smaller QD. This transition is denoted as |2> - |1>. While it may appear that the electron-hole recombination will adequately empty the lasing ground state, we do not believe the spontaneous emission decay, denoted by |2>-|1'> will effectively drain this level. This direct optical recombination process is slow, on the order of 1 ns, and even though electrons will be relaxing through the ground states of two QDs, not one, it will be too slow to effectively drain carriers. It is therefore necessary to couple the electron into a different reservoir than the vacuum electromagnetic field through radiation. We do this by adding a QW to the end of the asymmetric dot structure (Fig. 8). The lasing levels are shown in Fig. 9.

While the crystal growth of such a structure cannot currently be accomplished, the structure is conceptually realistic in a GaAs host with InAs QDs. A simulation based on this design has been made; the wavefunctions for an InAs coupled QDs structure is shown in Fig. 8. The device emits at approximately 7 THz.

Because of the coupling between the two QD, such a structure can be viewed as a QD *molecule* coupled to a reservoir (the QW). In such a structure a layer of such molecules are used. To increase the output, several layers of these QD molecules can be employed. As in the cascade quantum well laser, the quantum dot molecules can be vertically aligned and biased so that the larger dot aligns with a new smaller dot. The band
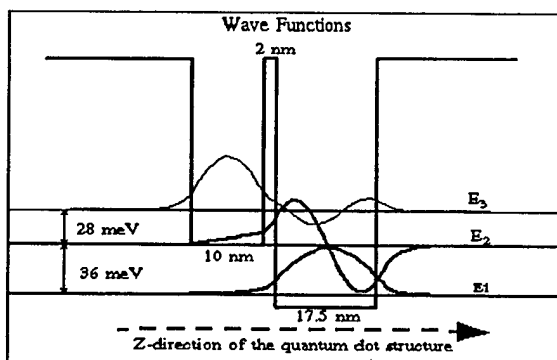

Fig. 10. Simulation of the wavefunctions and energy levels for a coupled QD structure. Radiative emission is from the |3>-|2> transition (courtesy of Cun-Zheng Ning, NASA Ames)

structure of such a device structure is shown in Figures 10 and 11. As in the QW cascade laser, the output of the ground state pumps the upper state of the next QD molecule and the QW reservoir is not necessary.
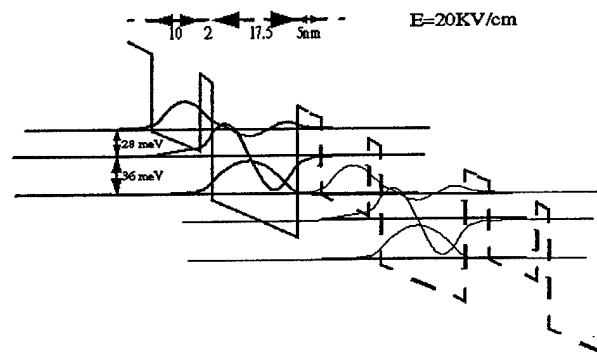
Fig. 11. The wavefunctions of a cascade of coupled QDs is shown, where the ground state of the higher potential molecule cascades to the upper state of the next molecule. (courtesy of Cun-Zheng Ning, NASA

In this cascade structure we must not only align the large and small QDs in each molecule, but also align the molecules into columns. Such a structure will be a sever test for emerging QD crystal growth techniques.

5.0 Quantum Dot Microcavity Terahertz source

A different approach from the coupled QD molecule (CAD) emitter source is a device structure designed around optical cavity coupling of the QD emitters. Unlike the CAD structure, these QDs are not quantum mechanically coupled. Here the cavity is principally used to provide optical feedback to QD radiative transition. However, the cavity additionally reduces the spontaneous emission lifetime of the radiative transition, increasing the spontaneous emission rate and reducing the lasing threshold. While the focus in the CAD structure is reducing the quasi-equilibrium ground state carrier density, here we focus on enhancing feedback. While the microdisk cavity is tuned to the radiative transition resonance, in a next-generation structure a second cavity can be formed vertically to enhance the ground state radiative decay rate and hence reduce the ground state quasi-equilibrium carrier density. Thus, the function of the primary cavity is to enhance feedback for stimulated emission in the intersublevel transition as well as to increase the spontaneous emission decay at this transition to increase the optical emission efficiency, while the second vertical cavity, tuned to the conduction-valence state transition, enhances spontaneous emission decay from the lasing ground state. Despite its apparent increased complexity such an addition is not difficult.

The QD microcavity THz emission source has two components: (1) An ensemble of QDs where the direct transition between the first excited state and the lowest lying state in the conduction band is used as the THz emission source; and (2) a passive cavity, the microdisk, which is used to couple light from the QD emitter source, provide enhanced spontaneous emission and feedback.

The terahertz microdisk has a diameter on the order of 300μm, yet the peak of the cavity mode is approximately 25μm from the disk edge. If QDs are uniformly distributed across the microdisk most of the QDs will not spatially couple to the cavity mode. In fact, measurement and theory by coworkers at Northwestern University show [17] that one explanation for the less than expected spontaneous emission enhancement is due to collected emission from QDs not spatially coupled to the cavity mode. Furthermore, the spatially uncoupled QDs towards the disk center trap carriers impeding carrier injection and diffusion into the cavity region. To reduce these effects we position QDs near the microdisk edge using selective area crystal growth.

We will break the discussion of this device into four parts: a description of the cavity effect and spontaneous emission; the mode distribution resulting from the microdisk cavity; placement of QDs selectively in the cavity mode; and rate equations describing the lasing process.

5.1 Enhancement of Spontaneously Emission in Microcavity

Spontaneous emission from a source such as a QW exciton, or atom is often thought of as an inherent property of the emitter, but is in fact a result of the interaction between the emitter dipole and the vacuum electromagnetic fields. Therefore, the radiation emitted from the source can be altered by suitably modifying the surrounding vacuum fields with a cavity. [18, 19] In 1946, Purcell first proposed the concept with respect to controlling the spontaneous emission (SE) rate of a quasi-monochromatic dipole by using a cavity to tailor the number of electromagnetic modes to which it is coupled. Later cavity quantum-electrodynamics (cavity-QED) has provided a firm theoretical and experimental basis for this idea. The ability to enhance the SE rate is so called Purcell Effect. Thus, besides the feedback to enhance gain, we can use our cavity to decrease the SE lifetime to reduce the lasing threshold.

First consider a general electric dipole transition given by the Fermi golden rule [20]

$$\frac{1}{\tau} = \frac{4\pi}{h} \rho(\omega) \left\langle \left| \vec{d} \cdot \vec{\varepsilon}(\vec{r}) \right|^2 \right\rangle, \qquad ($$

where τ is the spontaneous emission lifetime, $\vec{\varepsilon}(\vec{r})$ is the vacuum electric-field amplitude at the location $\vec{r}$ of the emitter and $\vec{d}$ is the electric dipole. $\rho(\omega)$ is the density of vacuum states at the emitter's angular frequency ω. However if the emitter is put into a cavity, the final density states $\rho(\omega)$ will be greatly modified and instead of being a constant value it is given by a normalized Lorentzian in the cavity case. So at resonance frequency ω_0, the density of modes could be very high depending the quality factor of the cavity.

Purcell originally considered this enhancement of spontaneously emission at the "weak coupling regime". That is, a localized dipole (wavelength λ_e, linewidth $\Delta\lambda_e$) placed on resonance with a single cavity mode (wavelength λ_c, linewidth $\Delta\lambda_c$, quality factor $Q = \lambda_c / \Delta\lambda_c$), and since $\Delta\lambda_e \ll \Delta\lambda_c$, the escape time of SE photons out of the cavity is much shorter than the radiative lifetime so re-absorption is negligible. In the weak-

coupling regime, the emitter interacts with a quasicontinuum of modes and the SE rate can be expressed using Fermi Golden rule. A simple derivation shows that the SE rate in the cavity mode, referenced to the total SE rate in a homogeneous medium, is given by the Purcell factor $F_p = 3Q\lambda_c^3 / 4\pi^2 n^3 V$, where n is the refractive index of the medium and V is the effective mode volume (V is given by the spatial integral of the vacuum field intensity for the cavity mode, divided by its maximum value). To obtain the maximum enhancement for a given by the Purcell factor, the emitter must be on exact resonance, located at the antinode of the vacuum field, with its dipole parallel to the vacuum electric field. Thus, the Purcell factor is the maximum enhancement from a cavity. But for a practical microcavity, the spontaneous emission enhancement can be expressed as

$$\frac{\gamma}{\gamma_0} = \frac{3Q(\lambda_c / n)^3}{4\pi^2 V} \frac{\Delta\lambda_c^2}{4(\lambda - \lambda_c)^2 + \Delta\lambda_c^2} \frac{|E(\vec{r})|^2}{|E_m|^2} 2\eta^2 = F_p g(\lambda) h(\vec{r}) 2\eta^2$$

where γ_0 is the spontaneous emission rate of dipole without the cavity; $E(\vec{r})$ is the electric field amplitude of the cavity mode at the position of the dipole emitter; $E_m = (h\nu / 2\varepsilon_0 n^2 V)^{1/2}$ is the maximum value of the electric field amplitude. The first term F_p is the Purcell factor. The second term $g(\lambda)$ and the third term $h(r)$ describe the spectral and spatial matching between the dipole emitter and the cavity mode. The factor of 2 comes from the two-fold degeneracy of the cavity mode. η describes the orientation match between the emitter dipole and the polarization of the cavity mode. We have shown the effect of the cavity on the spontaneous emission lifetime [21] and the that this effect is governed predominately by the spectral relationship to of the cavity and QD emitter in vertical, micropost cavities with cavity quality factors on the order of 1000 [22].

5.2 Calculation of THz optical mode in a microdisk

For ultralow laser thresholds, our microcavity design incorporates both high reflectivity and matching between a small gain volume and a single optical mode. The disk thickness is less than $\lambda / 2n_D$ (to guarantee single mode in the vertical direction), but larger than $\lambda / 4n_D$ (to guarantee one mode), and for most cases, it is selected to be $\lambda / 3n_D$. The index of refraction, n_D is calculated in the terahertz frequency range in the Appendix. Since we are interested in a wavelength of ~100 µm, the thickness $d \approx 10 \mu m$. Normally, the modes allowed in this kind of cavity are the combination of guided modes and non-guided modes, and the solution is very complicated. But in the case of R~λ, there are only several TE and TM modes allowed in the cavity. For example, we choose R=150 µm.

5.2.1 Allowed modes in the cavity:

The TE modes have lower threshold because of higher n_{eff}, so emission from TE modes will in general only be observed. We can divide the space into three regions: the guided region (in the disk), the evanescent region (outside disk, but close to the disk

edge) and the free-propagation region (far from the edge). Inside the disk, the field of TE_{ml} can be expressed as a Bessel function, J_m [23]:

$$
\begin{cases}
H_z = H_0 n_{eff} J_m(k_0 n_{eff}\rho)\cos(k_0\sqrt{n_D^2-n_{eff}^2}\,z)e^{im\theta} \\[2mm]
H_\rho = -H_0\sqrt{n_D^2-n_{eff}^2}\,J_m'(k_0 n_{eff}\rho)\sin(k_0\sqrt{n_D^2-n_{eff}^2}\,z)e^{im\theta} \\[2mm]
H_\theta = -iH_0 m\sqrt{n_D^2-n_{eff}^2}\,\dfrac{J_m(k_0 n_{eff}\rho)}{k_0 n_{eff}\rho}\sin(k_0\sqrt{n_D^2-n_{eff}^2}\,z)e^{im\theta}
\end{cases}
\tag{6}
$$

$$
\begin{cases}
E_z = 0 \\[2mm]
E_\rho = -\mu_0 c H_0 m\,\dfrac{J_m(k_0 n_{eff}\rho)}{k_0 n_{eff}\rho}\cos(k_0\sqrt{n_D^2-n_{eff}^2}\,z)e^{im\theta} \\[2mm]
E_\theta = -i\mu_0 c H_0 J_m'(k_0 n_{eff}\rho)\cos(k_0\sqrt{n_D^2-n_{eff}^2}\,z)e^{im\theta}
\end{cases}
\tag{7}
$$

$$ m \approx 2\pi R n_{eff}/\lambda = 18 $$

Here different mode index l corresponds to different effective index of refraction, n_{eff}. E and H are the electric and magnetic fields in polar coordinates, z, ρ, Θ, μ_0 is the permeability of free space, c the speed of light, k_0 the wave vector, and R is the disk radius. To obtain the allowed modes in the cavity, we solve the eigenfunction:

$$ \sqrt{n_D^2-n_{eff}^2}\,\tan\left[\frac{k_0 d}{2}\sqrt{n_D^2-n_{eff}^2}\right] = \sqrt{n_{eff}^2-1} $$

with the boundary condition:

$$ J_m(k_0 n_{eff} R) = 0 $$

We can now calculate the effective index and allowed wavelengths in the cavity. We express the quality factor Q (due to radiation loss only) as:

$$ Q = b\cdot\exp(2mJ),\ J = \tanh^{-1}(S) - S,\ \text{and}\ S = \sqrt{1-1/n_{eff}^2} $$

where $b\sim1/6.5$ in this formula is from an estimation of tunneling rates using the WKB approximation. We observe that: (1) a higher n_{eff} will lead to a higher Q and a lower threshold. This is the reason we only see TE modes instead of TM modes; (2) higher index, m means the field intensity will be closer to the edge, where the incidence angle is larger and so the radiation loss is smaller; (3) the FWHM of the edge-emission angle is estimated to be $2/\sqrt{m}$. So for higher order of TE_{ml}, we obtain a narrower edge-emission angle.

From the above analysis, we see that only the TE_{m1} or TE_{m2} mode is allowed in the cavity. Now, we can calculate λ, n_{eff} and Q for TE_{m1} ($m=17, 18, 19, 20, 21$) and TE_{m2} ($m=13, 14, 15, 16, 17$). The results are shown in Table 1. These absolute values determined by the calculations are only of relative meaning, because the cavity quality factor, Q will depend on the quality of the regrown cavity as well as the calculation

above. We see that the wavelengths of $TE_{m+4,1}$ and $TE_{m,2}$ modes are very close to each other.

	$TE_{17,1}$	$TE_{18,1}$	$TE_{19,1}$	$TE_{20,1}$	$TE_{21,1}$
λ (μm)	108.76	105.12	101.75	98.60	95.67
n_{eff}	2.5587	2.5940	2.6274	2.6592	2.6893
$Q(\times 10^9)$	1.3	7.7	47.2	296.6	1891.4
	$TE_{13,2}$	$TE_{14,2}$	$TE_{15,2}$	$TE_{16,2}$	$TE_{17,2}$
λ (μm)	109.52	105.58	101.95	98.60	95.49
n_{eff}	2.5514	2.5895	2.6254	2.6592	2.6911
$Q(\times 10^9)$	0.0055	0.0308	0.1764	1.0354	6.2040

Table 1. Calculated wavelength, effective index and quality factor for the first and second order TE modes in a microdisk cavity resonant in the 100 μm wavelength range.

An example of the microdisk cavity spatial mode distribution is shown in Fig. 12 for a microdisk resonant at approximately 100 μm. The spatial position of the cavity mode is approximately 25 μm from the microdisk edge.

5.3 QD placement in the microdisk

To align QDs near the microdisk perimeter, we chose to design a fabrication and crystal growth process where the QDs are selectively located along this perimeter. The process is achieved through an understanding of the strain-induced QD formation process. Since the QD formation relieves lattice mismatch stress by creating lateral free surface and the microdisk edge has a natural free surface, the microdisk edge is an optimum place for QD nucleation. In the normal QD formation process, when the strained material is deposited a thin region can be accommodated by planar biaxial compression, then after some thickness as been established the lowest energy state for the crystal is one with QDs. If there is a free surface to relax the strain material, the extra energy associated with creating lateral free surface is reduced: the extra lateral surface is already present. Thus, QDs will form near the microdisk perimeter first. Thus allows us to terminated the crystal growth after the QDs have formed on the microdisk perimeter but before they form on the interior region.

1. EPI LAYER

GaAs

Al$_{.75}$Ga$_{.25}$As

2. ETCH DISK

GaAs Substrate

3. QD REGROWTH - Top

InAs QDs

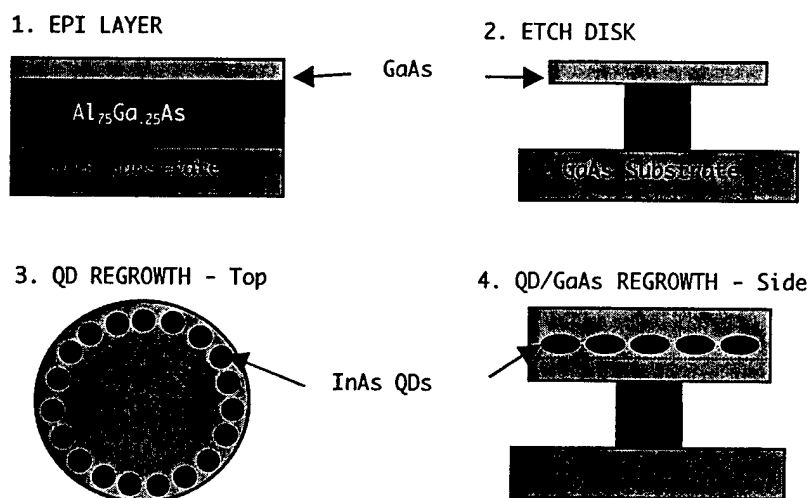**4. QD/GaAs REGROWTH - Side**

Fig. 13. Schematic of regrowth processing steps to form a microdisk cavity. (1) MBE is used to form the AlGaAs etch layer and approximately half the GaAs cavity. In (2) an isotropic etch etches down to the AlGaAs layer, after which a selective etch undercuts the AlGaAs to form the microdisk post. In (3), the regrowth is made after a final cleaning etch; QDs are aligned along the edge only, and (4) the GaAs top cavity is added.

The fabrication steps are shown in Fig. 13. First, the epitaxial structure containing the undercut region (AlGaAs) and 1/2 of the cavity region (GaAs) is made by MBE (Step 1 Fig. 13). In Step 2 lithography and wet-chemical etching is used to define the microdisk. Here, a non-selective etch is used to etch down to the GaAs substrate, then a selective etch is used to etch the AlGaAs and undercut the GaAs. In Step 3, Fig. 13 the processed

sample is re-inserted into the MBE machine and the InAs QD layer is made, and then covered with GaAs (Step 4).

The full process has already been demonstrated and is shown in Fig. 14 on the next page. In the figure atomic-force microscope (AFM) images show InAs QDs aligned at the edge of the microdisk. An AFM image of the disk is shown in Fig. 14b, where the light region at the disk edge is a near continuous, single chain of QDs. An enlargement of the image is shown in Fig. 14a. The QDs are approximately 40 nm in diameter. In Fig. 14c an AFM image of a micropost is shown. Here, there is no undercut. The image is clearer because the AFM is more stable without the less ridged undercut layer. Here, the microdisk is only 4 μm and the GaAs top-half of the cavity was not deposited in order to study the QD alignment. To fully investigate the structure we have designed the device to operate in near IR range with 900 nm wavelength operation. To design for this wavelength regime smaller disks are more useful. We are currently investigating the QD alignment process using the regrowth process on a variety of microdisk sizes.
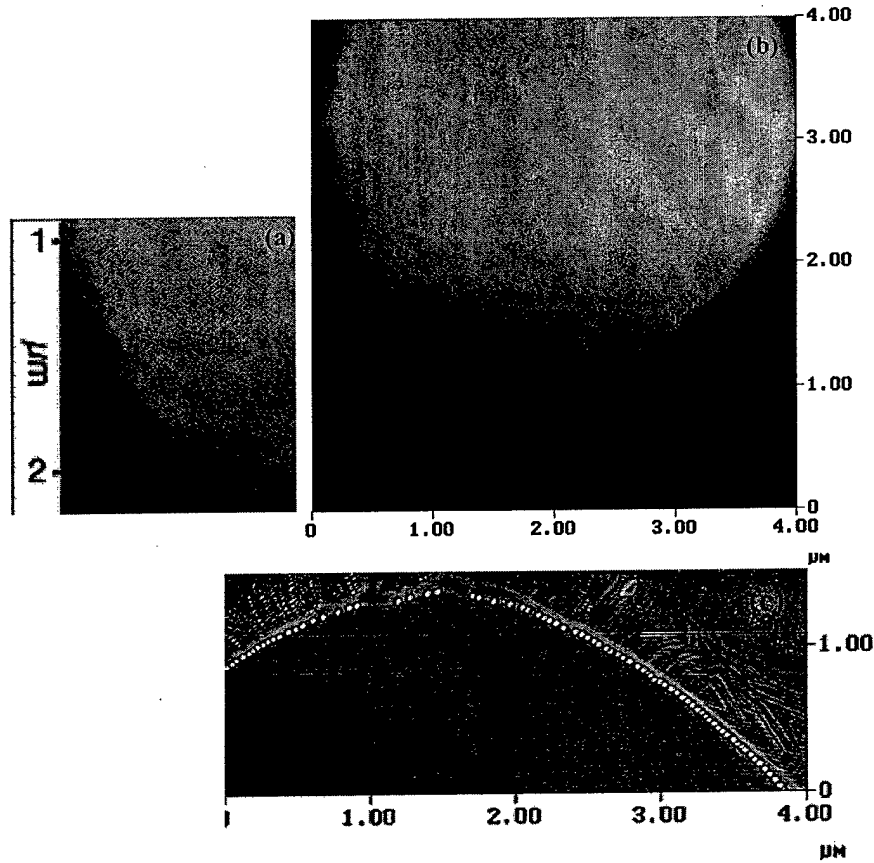
Fig. 14. AFM images of 4µm diameter GaAs micro-post, showing InAs QDs at the post edge and no QDs in the interior. (a,c) are magnified view of the post edge highlighting the QDs. Notice the very good edge alignment of QDs. Scale is in microns.

5.4 Tuning Optical Transitions for Lasing

The cavity is present for two purposes: (i) to capture photons, provide feedback and increase gain; and (ii) to enhance the spontaneous emission (SE) decay rate, γ, increasing the light output from the QD emitters. Point (i) is necessary in all semiconductor-based lasers. Point (ii) is helpful in all lasers but can be used in a subtler way in the intersublevel QD microcavity laser. In general, by coupling to electromagnetic cavity modes γ can be enhanced, reducing the onset to lasing. However, in designing the THz laser we must consider both the SE decay rate from the upper lasing level and the SE decay rate of the lower lasing level. In a band-to-band, electron-hole laser electrons and holes recombine producing a photons. Intersubband lasers are unipolar devices, excited state carriers decay into lower state carriers and do not annihilate each other. Therefore, the lasing threshold also depends the decay rate from the lasing ground state. In some cases such as in the cascade laser, the ground state population can be reduced by strong coupling to the LO phonon resonance.

22

At least initially, a choice must be made, to make the cavity resonant with the lasing wavelength or the lower state transition wavelength. To investigate options we have modeled the lasing threshold as a function of excited and ground state SE decay rates. We do this with a simple set of rate equations that include loss. The QD structure for the purposes of the simulation is shown in Fig. 15. In our model we refer to the lowest
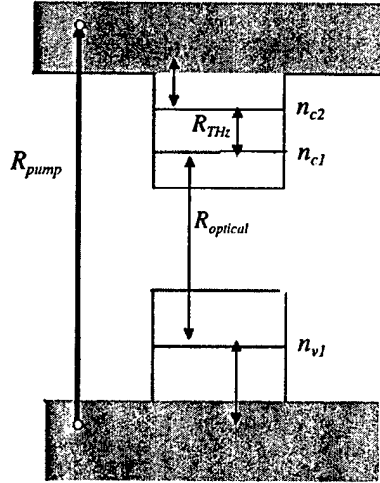

Fig. 15   Schematic of the QD used to establish a set of rate equations.

bound energy state of electron as n_{c1} and the next higher level is called n_{c2}. The only confined level of holes is n_{v1}. The electrons are pumped from very deep in valance band to very high in conduction band with a pumping rate of R_{pump} carriers per unit time per unit volume. The electrons and holes scatter down the bands and subsequently are captured in the confined electron and holes states, n_{c2}, n_{v1} respectively. Let us say that the corresponding capture rates are $R_{e,capture}$ and $R_{h,capture}$ carriers per unit time per unit volume respectively. Hence we can write a simple set of rate equations for describing the time evolution of carrier density in the three confined levels of QDs:

$$\frac{dn_{c1}}{dt} = R_{THz} + R_{non-radiative} - R_{Optical}$$

$$\frac{dn_{c2}}{dt} = R_{e,capture} - R_{THz} - R_{non-radiative}$$

$$\frac{dn_{v1}}{dt} = R_{Optical} - R_{h,capture}$$ (11)

where, R_{THz} is the net rate of the intersublevel THz transition – the rate at which electrons in the higher energy level n_{c2} drop to an empty lower energy level n_{c1}, emitting a THz photon (either spontaneously or by stimulation), minus the rate at which electrons in the lower energy levels n_{c2} absorb a THz photon and jumps to an empty higher energy level n_{c2}. Adding all three components, R_{THz} can be written as:

$$R_{THz} = \frac{(n_{c2})(n_{QD} - n_{c1})}{\tau_{c2,c1}} + \frac{(n_{p,THz})(n_{c2} - n_{c1})}{\tau_{c2,c1}}$$ (12)

Similarly, $R_{Optical}$ is the net rate of confined conduction band-to-valence state transitions that absorb or emit a photon. This is the more typical interband transition. It is equal to the rate at which electrons in the lower energy level of the conduction band (n_{cl}) drop to an empty energy level in the valence band (n_{vl}), emitting an optical photon (either spontaneously or by stimulation), minus the rate at which electrons in the valance band energy level n_{vl} absorbs an optical photon and jumps to an empty conduction band level n_{cl}. Adding all three components $R_{Optical}$ can be written as:

$$R_{Optical} = \frac{(n_{cl})(n_{QD} - n_{vl})}{\tau_{c2,cl}} + \frac{(n_{p,Optical})(n_{cl} - n_{vl})}{\tau_{cl,vl}} \tag{13}$$

$n_{p,THz}$, and $n_{p,Optical}$ are the photon densities in the THz mode and optical mode of the cavity. This cavity can be singly resonant at the THz frequency, or doubly resonant to enhance the optical transition rate. $\tau_{c2,cl}$ is the spontaneous emission lifetime. $R_{non-radiative}$ is the rate of non radiative intersublevel transitions.

Since the rate of change of the carrier densities in all three confined energy levels strongly depends on the densities of photons in both the cavity modes, it becomes necessary to know how the photon densities themselves evolve with time. The time evolution of photon densities in the two cavity modes can be described by:

$$\frac{dn_{p,THz}}{dt} = -\frac{\omega_{THz}}{Q_{THz}} n_{p,THz} + R_{THz} \tag{14}$$

$$\frac{dn_{p,Optical}}{dt} = -\frac{\omega_{Optical}}{Q_{Optical}} n_{p,Optical} + R_{Optical} \tag{15}$$

where, ω_{THz} and $\omega_{Optical}$ are the resonant frequencies of THz and optical modes. Q_{THz}
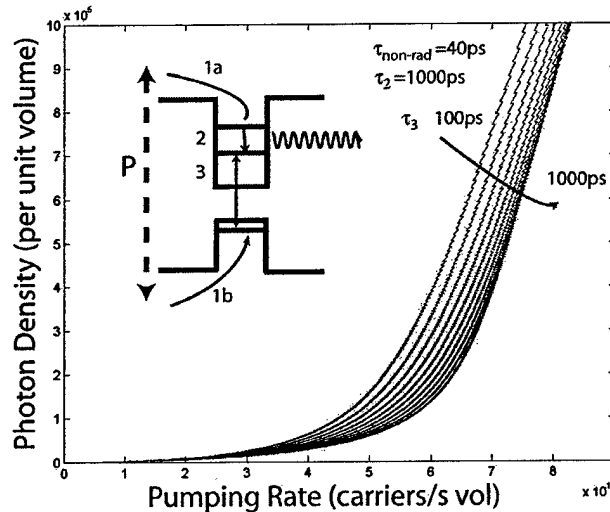

Fig. 16. Results of rate equations modeling of QD intersublevel laser. The lasing level is 2, and the non-radiative lifetime is set at 1/25 of the SE lifetime of the lasing state. The ground state lifetime is varied and clamps the threshold when approaching the SE lifetime of the lasing state.

and $Q_{Optical}$ are the corresponding Q-factors. These coupled rate equations for carriers and photons in two modes can easily be simulated. The simulation is used to predict the required threshold pumping rate.

For the purposes of the simulation, we set the loss rate higher than the SE rate for any states to model the high losses in the THz range. A set of L-I curves is shown in Fig. 16. The horizontal axis is the pumping rate of electron-hole pairs into the bulk crystal, and the non-radiative loss lifetime is set at 40ps, the upper state, THz SE lifetime is 1000ps and the lower, optical SE lifetime varies between 100 and 1000 ps. As the lower state lifetime increases the lasing threshold becomes clamped because the lower state cannot remove carriers as fast as they enter the upper state. This is highlighted in Fig. 17, where
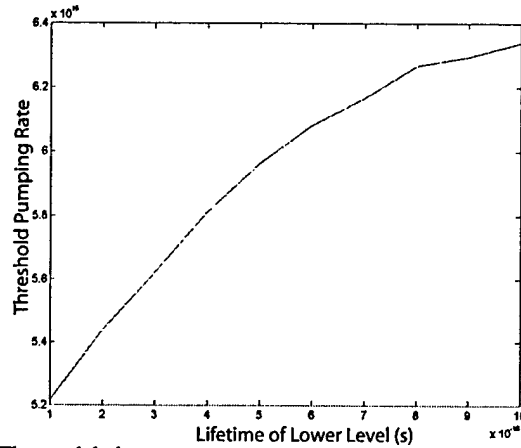

Fig. 17. The modeled pump rate necessary to achieve lasing is plotted against the lifetime of the lower level quantum dot state. As the lifetime of this state increases, so does the pump rate necessary for lasing.

the pumping rate required for lasing (the threshold rate) is plotted against the lifetime of the lower state. If the upper state SE lifetime is sufficiently small, the microdisk must be designed to be resonant with lower state wavelength. Conversely, if the upper state SE lifetime is long compared to the lower state SE lifetime, the cavity must be designed to be resonant with the upper state.

We have made single QD SE lifetime measurements of the ground state emission. An example is shown in Fig. 18. The QD is optically pumped with energy above the GaAs bandgap. The quick rise time indicates carriers relax to the ground state remarkably fast. In Fig. 18 the rise time of the ground state is approximately 40 ps. The SE lifetime of the ground state however is approximately 500 ps. Thus, our initial conclusion is that the ground state SE lifetime may limit the threshold if adjustments to our cavity design are not made. It is possible that the cavity could be resonant at both the intersublevel transition and the ground state band-to-band transition however, while the microdisk will have more resonances in the band-to-band region it is unlike that these resonances will align with both transitions of the QD. It is possible to incorporate a vertical cavity structure into the microdisk cavity, where the vertical cavity is composed of distributive-Bragg reflector (DBR) mirror pairs tuned to the ground state transition
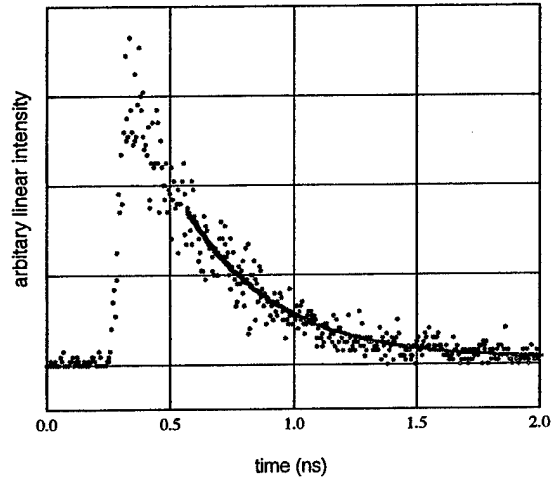
Fig. 18. Spontaneous emission lifetime of the ground state in a single QD at 4K. The fast rise time indicates fast relaxation into the ground. The ground state lifetime is approximately 500 ps.

(approximately wavelength, 1 μm). This should not affect the microdisk cavity, which remains resonant in the THz range. A schematic of this proposed structure is shown in Fig. 19.
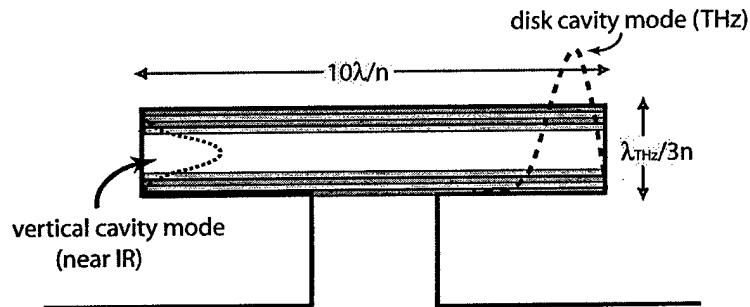

Fig. 19. Microdisk cavity with vertical, planar distributive-Bragg reflector (DBR) mirror pairs. The microdisk cavity is resonant in the terahertz frequency range, and couples to the intersublevel QD transition. The vertical cavity is resonant in the near-IR and couples to the conduction-valence transition. The vertical cavity reduces the spontaneous emission lifetime, and removes carriers from the lasing ground state.

26

Appendix: Calculation of the Refractive Index

From E.D. Palik, Handbook of Optical Constants of Solids, Academic, New York, 1985,

the refractive index of GaAs as a function of frequency is:

$$n^2 = 1 + \frac{A}{\pi}\ln\frac{E_1^2 - (\hbar\omega)^2}{E_0^2 - (\hbar\omega)^2} + \frac{G_1}{E_1^2 - (\hbar\omega)^2} + \frac{G_2}{E_2^2 - (\hbar\omega)^2} + \frac{G_3}{E_3^2 - (\hbar\omega)^2}$$

where $E_0 = 1.428eV$, $E_1 = 3.0eV$, $G_1 = 39.194eV^2$, $E_2 = 5.1eV$, $G_2 = 136.08eV^2$, $A = 0.5858$
$E_3 = 0.0333eV$, $G_3 = 0.00218eV^2$,

So the calculated n=3.6257 for a wavelength of 100 μm.

References

[1] J. Kono, S.T. Lee, M.S. Salib, G.S. Herold, A. Petrou, and B.D. McCombe, Phys. Rev. B **52**, R8654 (1995).

[2] J. Cerne, J. Kono, M.S. Sherwin, M. Sundaram, A.C. Gossard, and G. E. W. Bauer, Phys. Rev. Lett. **77**, 1131 (1996).

[3] Y. Naveh and B. Laikhtman, Phys. Rev. Lett. **77**, 900 (1996).

[4] D. Woolard, *et. al.*, Phys. Rev. E **65**, 1903-1914 (2002).

[5] M. Zandian, J. M. Arias, R. Zucca, R. V. Gil, and S. H. Shin, Appl. Phys. Lett. **59**, 102 (1991); R. Zucca, M. Zandian, J. M. Arias and R. Gil, SPIE Proc., **1634**, 161 (1992); J. M. Arias, M. Zandian, R. Zucca, and J. Singh, Semicond. Sci. Technol., **8**, S 255 (1993).

[6] J. Faist, F. Capasso, D. L. Sirtori, A. L. Hutchinson, and A. Y. Cho, Science **264**, 553 (1994).

[7] M. Rochat, *et al.*, Appl. Phys. Lett. **81** 1383 (2002).

[8] E. R. Brown, *et al.*, Appl. Phys. Lett. **58** 2291 (1991).

[9] R. A. Smith, *Semiconductors, Second Edition,* Cambridge University Press, Cambridge (1978).

[10] H. Y. Fan, Rep. Progr. Phys. **19**, 107 (1956).

[11] W. P. Dumke, Phys. Rev. **124**, 1813 (1961).

[12] A. R. Adams, E. P. O'Reilly and M. Silver, *Strained Layer Quantum Well Lasers,* in *Semiconductor Lasers, Vol. I,* edited by E. Kapon, Academic Press, San Deigo, CA (1999).

[13] H. Cao, J. Y. Xu, W. H. Xiang, Y. Ma, S. –H. Chang, S. T. Ho and G. S. Solomon, Appl. Phys. Lett. **76** 3519 (2000).

[14] G. S. Solomon, J. A. Trezza, A. F. Marshall, and J. S. Harris, Jr., Phys. Rev. Lett. **76**, 952, 1996.

[15] M. Bayer, P. Hawrylak, K. Hinzer, S. Fafard, M. Korkusinski, R. Wasilewski, O. Stern, A. Forchel, Science **291**; 451 (2001).

[16] G. S. Solomon, S. Komarov , J. S. Harris, Jr. and Y. Yamamoto, J. Cryst. Growth, **175/176**, 707 (1996).

[17] W. Fang, J. Y. Xu, A. Yamilov, H. Cao, Y. Ma, S. T. Ho and G. S. Solomon, Opt. Lett. **27**, 948 (2002).

[18] E. M. Purcell, Phys. Rev. 69, 681 (1946).

[19] Drexhage, K. H. *Progress in Optics* (ed. by Wolfe, E., Vol. XII, 165-232 North-Holland, Amsterdam, 1974).

[20] J. M. Gerard, Phys. Rev. Lett. **81**, 1110 (1998).

[21] G. S. Solomon, M. Pelton, and Y. Yamamoto, Phys. Rev. Lett. **86**, 3903 (2001).

[22] G. S. Solomon, M. Pelton, and Y. Yamamoto, Phys. Rev. Lett., accepted for publication (2003).

[23] Ruo Peng Wang, *et al.*, J. .Appl. Phys. **81**, 391 (1997).